

Nuclear charge and neutron radii and nuclear matter: trend analysis

P.-G. Reinhard¹ and W. Nazarewicz^{2,3}

¹*Institut für Theoretische Physik, Universität Erlangen, D-91054 Erlangen, Germany*

²*Department of Physics and Astronomy and NSCL/FRIB Laboratory,
Michigan State University, East Lansing, Michigan 48824, USA*

³*Institute of Theoretical Physics, Faculty of Physics, University of Warsaw, Warsaw, Poland*
(Dated: January 26, 2016)

Background: Radii of charge and neutron distributions are fundamental nuclear properties. They depend on both nuclear interaction parameters related to the equation of state of infinite nuclear matter and on quantal shell effects, which are strongly impacted by the presence of nuclear surface.

Purpose: In this work, by studying the dependence of charge and neutron radii, and neutron skin, on nuclear matter parameters, we assess different mechanisms that drive nuclear sizes.

Method: We apply nuclear density functional theory using a family of Skyrme functionals obtained by means of different optimization protocols targeting specific nuclear properties. By performing the Monte-Carlo sampling of reasonable functionals around the optimal parametrization, we study correlations between nuclear matter parameters and observables characterizing charge and neutron distributions of spherical closed-shell nuclei ^{48}Ca , ^{208}Pb , and ^{298}Fl .

Results: We demonstrate the existence of the strong converse relation between the nuclear charge radii and the saturation density of symmetric nuclear matter ρ_0 , and also between the neutron skins and the slope of the symmetry energy L . For functionals optimized to experimental binding energies only, proton and neutron radii are weakly correlated due to canceling trends from different nuclear matter parameters.

Conclusion: We show that by requiring that the nuclear functional reproduces the empirical saturation point of symmetric nuclear matter practically fixes the charge (or proton) radii, and vice versa. This explains the recent results of ab-initio calculations with two-nucleon and three-nucleon forces optimized simultaneously to binding energies and radii of selected nuclei. The neutron skin uncertainty primarily depends on the slope of the symmetry energy. Consequently, imposing a constraint on both ρ_0 and L practically determines the nuclear size, modulo small variations due to shell effects.

PACS numbers: 21.10.Gv, 21.60.Jz, 21.65.Cd, 21.65.Mn

Introduction – Radii of proton (or charge) and neutron distributions in atomic nuclei are key observables that can be directly related to fundamental properties of nuclear matter and to the nature of nuclear force (see Ref. [1] and references quoted therein). In heavy nuclei, the excess of neutrons gives rise to a neutron skin, characterized by the neutron distribution extending beyond the proton distribution. The neutron skin has been found to correlate with a number of observables in finite nuclei and nuclear and neutron matter [2–23]; hence, it beautifully links finite nuclei with extended nuclear matter found, e.g., in neutron stars.

The goal of this study is to understand the relations between proton and neutron radii, and neutron skins using nuclear density functional theory (DFT) [24], which is a tool of choice in microscopic studies of complex nuclei. In particular, we inspect the relations between nuclear matter parameters characterizing effective interactions, here represented by Skyrme energy density functionals (EDFs) adjusted to experimental data using different optimization strategies. By means of the statistical covariance technique, we quantify the intricate relation between the proton and neutron radius, and explain the recent results of a comparative study for ^{48}Ca [1].

The strategy – To explore the correlations between neutron radius, proton radius, and neutron skin, we use

the tools of linear regression based on least-squares (χ^2), which were adopted recently in the nuclear context in Refs. [11, 25–35]. In particular, we use here analysis of covariances (statistical correlations) between observables, error propagation, and an exploration of χ^2 in the vicinity of the best fit. Our starting point is the parametrization SV-min [36] optimized to the pool of ground-state data. The corresponding set of fit-observables had been carefully selected to include only nuclei which have very small correlation corrections [37] and thus can be described reliably within a standard single-reference nuclear DFT. Since the set of fit-observables constraining SV-min contains also information on radii deduced from the charge form factor data [38, 39], this makes this EDF parametrization less useful for the present study, whose objective is to explore correlations with charge radii. Indeed, one should not trust correlations for an observable which was included in the fit as the behavior of χ^2 in the direction of this observable is usually very rigid [34]. To provide sufficient leeway to explore radii, the radius information should be excluded from the fit. Thus we consider here the SV-min set of fit observables excluding the data on radii. This leaves in the fit pool only energy information, namely binding energies of sixty semi-magic nuclei, pairing gaps from odd-even binding energy differences for long isotopic and isotonic chains, and a few

selected spin-orbit splitting in doubly-magic nuclei. (For details of the fit data, see Tables III and IV of Ref. [36].) The EDF optimized to this dataset is referred to as SV-E in the following. This parametrization and the effect of omission of radius information had been discussed in Refs. [31, 35]. Here, we use SV-E merely as a tool to explore radius correlations.

The Skyrme EDF is described by means of 14 parameters. The pairing functional contains three parameters: proton and neutron pairing strengths and a parameter defining the density dependence. Two parameters are used for calibrating the isoscalar and isovector spin-orbit force [40]. Two parameters are necessary to tune the surface energy. Finally, there remain seven parameters characterizing volume properties. These are fully equivalent to key properties of uniform symmetric nuclear matter at equilibrium, called henceforth Nuclear Matter Parameters (NMP). Those are: the saturation density ρ_0 and energy-per-nucleon E/A , of symmetric nuclear matter; incompressibility K and effective mass m^*/m characterizing the isoscalar response; and symmetry energy J , slope of symmetry energy L , and Thomas-Reiche-Kuhn sum rule enhancement factor κ_{TRK} characterizing the isovector response. Those NMP will be used in the following to sort the results and establish correlations with radii.

For the following analysis, we employ three strategies. First, we employ the standard covariance analysis explained, e.g., in Refs. [29, 41]. Here, we compute the covariance matrix for SV-E and use it to deduce the covariances (correlations) between the observables of interest. Second, we explore explicitly the hyper-surface of “reasonable parametrizations” in the vicinity of the SV-E parameter set. Recall that, around the minimum of χ^2 parametrizations are distributed with probability $W(\mathbf{p}) \propto \exp[-\chi^2(\mathbf{p})]$ where \mathbf{p} stands for the (twelve) free parameters of the model and \mathbf{p}_0 is the SV-E parameter set. We sample this distribution in a Monte-Carlo fashion by representing it by an ensemble of 2000 parametrizations. Thereby, we confine the search to the space of \mathbf{p} with $W(\mathbf{p}) > 1/2$ to avoid excessive amount of unsuccessful hits in the large parameter space. The close vicinity of \mathbf{p}_0 suffices for the present purposes as it contains all crucial trends and correlations. (For more discussion of such strategy, see Ref. [30].) Finally, we employ the rules of error propagation in the context of χ^2 fits. We use this to explore the sensitivity of the radii to NMP by constraining the fit by selected NMP (while using always exactly the same pool of fit observables) and studying resulting changes in the uncertainties of the predicted radii. The chosen NMP is always fixed at the SV-E value. This means that the optimal parameters \mathbf{p}_0 remain the same. What changes are allowed variations in \mathbf{p} which, in turn, impact the extrapolation uncertainties. We shall see a strong correlation if one NMP reduces significantly the uncertainty of an observable.

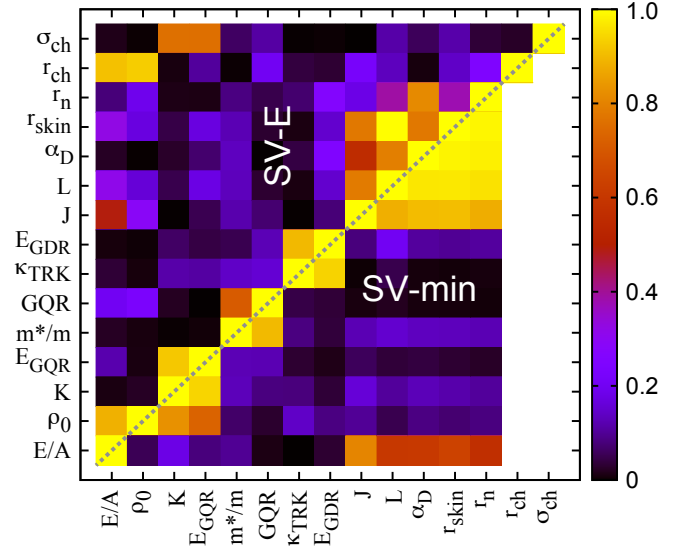


FIG. 1. (Color online) Covariance matrices for a selection of observables and NMP computed with SV-min [36] (below the diagonal) and SV-E [31, 35] (above the diagonal). Nuclear observables (in ^{208}Pb) are: charge surface thickness σ_{ch} ; root-mean-square (rms) charge radius r_{ch} ; rms neutron radius r_{n} ; neutron skin r_{skin} ; electric dipole polarizability α_{D} ; and giant resonance energies E_{GDR} and E_{GMR} . The NMP corresponding to the symmetric nuclear matter include: incompressibility K , symmetry energy J , symmetry energy slope L , isoscalar effective mass m^*/m ; TRK sum-rule enhancement κ_{TRK} ; and density ρ_0 and energy E/A at the saturation point. The correlations with the charge form factor data σ_{ch} and r_{ch} are not shown for SV-min as these quantities were included in the corresponding set of fit-observables.

Results – We begin by inspecting in Fig. 1 the covariance matrices of SV-min and SV-E. The general pattern seen in Fig. 1 was discussed in Refs. [31, 35]. The strong correlations between the isovector indicators (symmetry energy J , symmetry energy slope L , rms neutron radius r_{n} , neutron skin $r_{\text{skin}} = r_{\text{n}} - r_{\text{p}}$, and electric dipole polarizability α_{D}) seen in SV-min become significantly degraded in SV-E, with the strongest remaining correlation being that between r_{skin} and L . Indeed, as concluded in [31, 35] L is the leading bulk parameter for isovector static response. The charge radius r_{ch} in SV-E correlates very well with the saturation point (ρ_0 and E/A) but rather poorly with other quantities. On the other hand, the neutron radius in SV-E has a reasonable correlation with α_{D} but it is hardly correlated with r_{ch} , ρ_0 , and E/A .

In the following, we shall test the robustness of the correlations $r_{\text{ch}} \leftrightarrow \rho_0$ and $r_{\text{skin}} \leftrightarrow L$ by inspecting trends in ^{48}Ca , ^{208}Pb , and also in ^{298}Fl ($Z = 114, N = 184$) – a spherical superheavy nucleus, in which the leptodermous expansion is expected to work best [42]. By considering a medium-mass, heavy, and superheavy nucleus, we can assess whether finite-size (or shell) effects do not cloud our conclusions. To illustrate the impact of NMP on

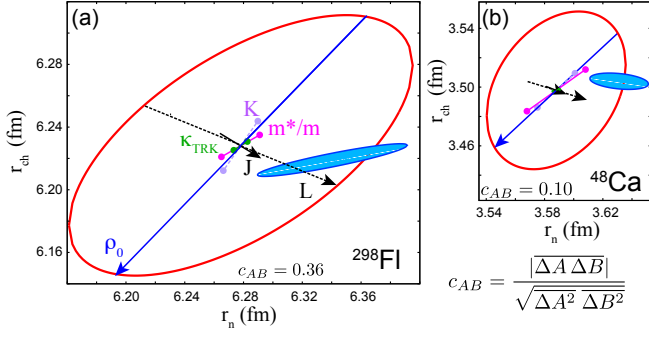


FIG. 2. (Color online) Variance ellipsoids with SV-E in the $(r_{\text{ch}}, r_{\text{n}})$ -plane for ^{298}Fl (a) and ^{48}Ca (b). The arrows/segments indicate the direction of changing radii when varying one NMP as indicated. Their lengths represent the magnitude of corresponding variations. The narrow ellipsoids mark the SV-min results. The correlation coefficient c_{AB} between r_{ch} and r_{n} is indicated in both cases.

r_{ch} and r_{n} , Fig. 2 shows the SV-E variance ellipsoids in the $(r_{\text{ch}}, r_{\text{n}})$ -plane. Consistent with results displayed in Fig. 1, the variance ellipsoids are primarily impacted by the variations in the directions of ρ_0 and L . The impact of other NMP is much less. Interestingly, the directions of trends due to changes in ρ_0 and L (marked by arrows) are fairly different. That is, increasing ρ_0 decreases both r_{ch} and r_{n} , as expected from the relation between the density and the Wigner-Seitz radius. On the other hand, increasing L decreases r_{ch} and increases r_{n} . The trend due to changes in J generally follows that of L , albeit with a much smaller magnitude. Due to the compensating trends, the correlation $r_{\text{ch}} \leftrightarrow r_{\text{n}}$ is very small; namely, it is $c_{AB}=0.10$ for ^{48}Ca and it increases to $c_{AB}=0.36$ for ^{298}Fl . This illustrates that these two quantities are not strongly coupled by the Skyrme EDF. Figure 2 also shows the corresponding SV-min ellipsoids (narrow, blue). As expected, these are very narrow in the direction of r_{ch} , as this quantity has been constrained in the fit of SV-min. On the other hand, the uncertainty in r_{n} is significant.

Figures 3-5 display systematic trends obtained with the ensemble of 2000 parametrizations around SV-E. These results fully confirm our previous findings. Namely, ρ_0 , L , and J nicely correlate with rms radii and neutron skin while K , m^*/m , and κ_{TRK} do not. The behavior of radii in Fig. 4 is consistent with the trends in Fig. 2 for the variance ellipsoids. It is interesting to notice that for a fixed value of ρ_0 , the spread of the proton (or charge) radii is fairly narrow, while it is significantly broader for the neutron radii. Finally, as shown in Fig. 5, neutron skins correlate well with J but their correlation with L is superior, especially for heavy nuclei.

The strong $r_{\text{ch}} \leftrightarrow \rho_0$ and $r_{\text{skin}} \leftrightarrow L$ relations can be quantified by studying the predicted uncertainties on radii and skins. To this end, we carry out additional EDF

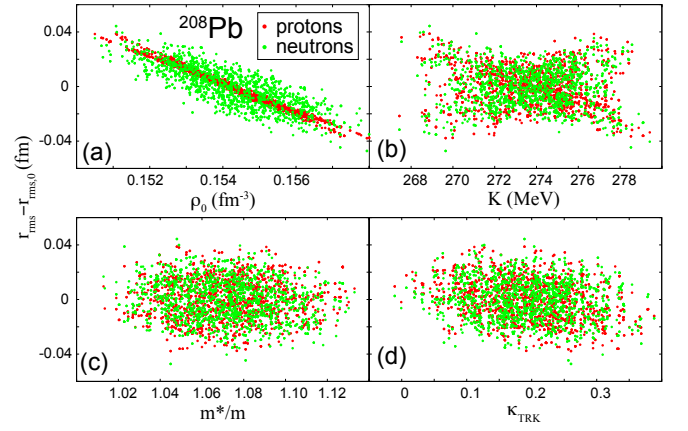


FIG. 3. (Color online) Proton (red), and neutron (green) rms radii in ^{208}Pb with respect to the SV-E values from the ensemble of 2000 parametrizations in the vicinity of the optimal fit SV-E drawn versus different NMP: ρ_0 (a), K (b), m^*/m (c), and κ_{TRK} (d).

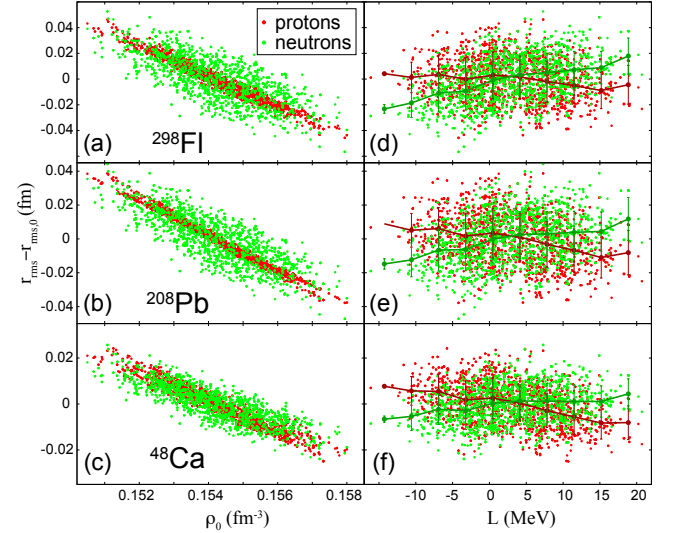


FIG. 4. (Color online) Similar as in Fig. 3 but versus ρ_0 (left) and L (right) for ^{298}Fl (top), ^{208}Pb (middle), and ^{48}Ca (bottom). To illustrate the trends, the right panels show also averages and variances of radii taken over bins in L .

optimizations by using the same pool of fit-observables as SV-E but constraining one or two NMP at the values given by SV-E. Figure 6(e) illustrates the $r_{\text{ch}} \leftrightarrow \rho_0$ correspondence: by constraining the saturation density ρ_0 the theoretical uncertainty on r_{ch} is reduced by $\sim 50\%$. Even more striking is the result for the neutron skin in Fig. 6(c): constraining L in the EDF optimization practically fixes r_{skin} . The correlation $r_{\text{skin}} \leftrightarrow L$ follows from the leptodermous analysis [10], which shows that $r_{\text{skin}} \propto L/J$.

The surface thickness parameters displayed in Figs. 6(a) and (b) are hardly affected by precise knowledge of ρ_0 , L , and J . What about the neutron radii? As

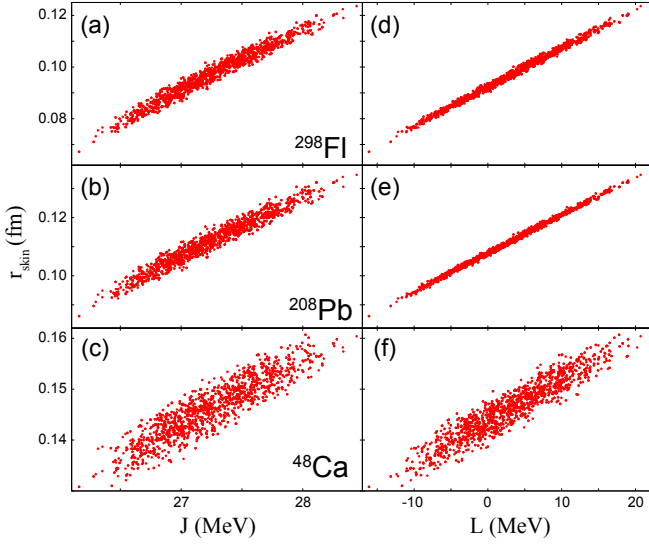


FIG. 5. (Color online) Neutron skins from the ensemble of 2000 parametrizations in the vicinity of the optimal fit SV-E versus J (left) and L (right) for the three nuclei under consideration.

seen in Fig. 6(d), fixing ρ_0 or L helps reducing theoretical uncertainty slightly, but it is simultaneous knowledge of ρ_0 and L that helps reducing the error on r_n . But this can be viewed as a secondary effect of the $r_{ch} \leftrightarrow \rho_0$ and $r_{skin} \leftrightarrow L$ relations. Indeed, $r_n = r_n + r_{skin}$; hence, $\Delta r_n = \Delta r_n + \Delta r_{skin}$. The uncertainty of the first term is reduced by precise information on ρ_0 while the error on the second term is reduced by our knowledge of L .

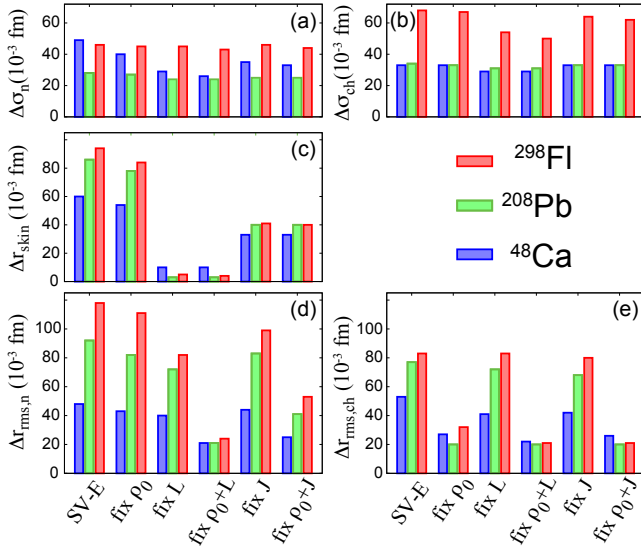


FIG. 6. (Color online) Uncertainties in the predictions of rms neutron and charge radii (bottom), neutron skins (middle), and surface thicknesses (top) for different EDF fits. The reference EDF is SV-E. Other EDF fits use the same pool of fit-observables as SV-E but constrain one or two NMP, as indicated, at the SV-E values.

Figure 6 also shows results with EDFc obtained by constraining the symmetry energy J . As discussed earlier, the trends due to J follow those triggered by variations in L , but they are weaker. This is because our current knowledge of J is much better than that of L . For instance, the values of J are 31 ± 2 MeV in SV-min and 27 ± 2 MeV in SV-E (a mere 6-7% error), while the values of L in SV-min and SV-E are 45 ± 26 MeV and 3 ± 63 MeV, respectively (i.e., they are very uncertain).

Conclusion – By using the statistical tools of linear regression, we studied radii of neutron and proton distributions within the Skyrme-DFT framework. The analysis was carried out for the spherical closed-shell nuclei ^{48}Ca , ^{208}Pb , and ^{298}Fl , and the results turned out to weakly depend on the system considered, i.e., shell effects. The main conclusion of our study is that there exist, at least within the Skyrme-DFT theory, converse relations between radii in finite nuclei and parameters ρ_0 and L characterizing the equation of state of uniform nuclear matter: $r_{ch} \leftrightarrow \rho_0$ and $r_{skin} \leftrightarrow L$. For instance, by including charge radii in a set of fit-observables, as done for the majority of realistic Skyrme EDFs [24], one practically fixes the saturation density ρ_0 . Indeed, by adding the charge form factor information to the set of fit-observables of SV-E, one reduces the theoretical uncertainty on ρ_0 by a factor of 7 (from $\rho_0 = 0.1542 \pm 0.0076 \text{ fm}^{-3}$ in SV-E to $\rho_0 = 0.1611 \pm 0.0011 \text{ fm}^{-3}$ in SV-min). Recently, a similar conclusion has been reached in ab-initio calculations based on a chiral interaction NNLO_{sat} optimized simultaneously to low-energy nucleon-nucleon scattering data, as well as binding energies and radii of finite nuclei [43]. Here, the use of data on charge radii was crucial for reproducing the empirical saturation point of symmetric nuclear matter.

By inspecting various, often competing, trends in Fig. 2 one is tempted to conclude that the $r_n \leftrightarrow r_p$ relation is fairly complex. Namely, various trends are possible when moving along ‘a’ trajectory in a parameter space $\{p\}$. In this respect, we suggest the two directions that are most important are given by the variations in ρ_0 and L . Our analysis, in particular the results shown in Fig. 6 suggest that reducing the uncertainty on L would lead to a dramatic improvement in our knowledge of neutron skins and neutron radii. This is consistent with the findings of Ref. [18] that the slope of the symmetry energy L is the single main contributor to the statistical uncertainty of r_{skin} . Conversely, by using the precise information on neutron skins (when available) should allow to improve our knowledge of L , hence the neutron matter equation of state.

Finally, we conclude that while adding a constraint on experimental charge radii gives rise to EDFs that are of high fidelity with respect to proton radii, the corresponding model uncertainties on the neutron radii due to our poor knowledge of L are still appreciable [18]. This explains the Skyrme-DFT results in a recent comparative

study for ^{48}Ca [1].

This material is based upon work supported by the U.S. Department of Energy, Office of Science, Office of Nuclear Physics under award numbers de-sc0013365 (Michigan State University) and de-sc0008511 (NUCLEI SciDAC-3 collaboration); by the German ministry of Science and Technology, grant number 05P12RFFTG; by the Deutsche Forschungsgemeinschaft, grant number RE 322-14/1; and by Bundesministerium für Bildung und Forschung (BMBF) under contract number 05P09RFFTB.

-
- [1] G. Hagen, A. Ekström, C. Forssén, G. R. Jansen, W. Nazarewicz, T. Papenbrock, K. A. Wendt, S. Bacca, N. Barnea, B. Carlsson, C. Drischler, K. Hebeler, M. Hjorth-Jensen, M. Miorelli, G. Orlandini, A. Schwenk, and J. Simonis, *Nat. Phys.* **advance online publication**, (2015).
 - [2] F. Tondeur, M. Brack, M. Farine, and J. Pearson, *Nucl. Phys. A* **420**, 297 (1984).
 - [3] P.-G. Reinhard, *Nucl. Phys. A* **649**, 305c (1999).
 - [4] B. Alex Brown, *Phys. Rev. Lett.* **85**, 5296 (2000).
 - [5] C. J. Horowitz and J. Piekarewicz, *Phys. Rev. Lett.* **86**, 5647 (2001).
 - [6] C. J. Horowitz and J. Piekarewicz, *Phys. Rev. C* **64**, 062802 (2001).
 - [7] S. Typel and B. A. Brown, *Phys. Rev. C* **64**, 027302 (2001).
 - [8] R. Furnstahl, *Nucl. Phys. A* **706**, 85 (2002).
 - [9] F. Sammarruca and P. Liu, *Phys. Rev. C* **79**, 057301 (2009).
 - [10] M. Centelles, X. Roca-Maza, X. Viñas, and M. Warda, *Phys. Rev. Lett.* **102**, 122502 (2009).
 - [11] P.-G. Reinhard and W. Nazarewicz, *Phys. Rev. C* **81**, 051303(R) (2010).
 - [12] X. Roca-Maza, M. Centelles, X. Viñas, and M. Warda, *Phys. Rev. Lett.* **106**, 252501 (2011).
 - [13] J. Piekarewicz, B. K. Agrawal, G. Colò, W. Nazarewicz, N. Paar, P.-G. Reinhard, X. Roca-Maza, and D. Vretenar, *Phys. Rev. C* **85**, 041302 (2012).
 - [14] D. J. Agrawal, B.K. and S. Samaddar, *Phys. Lett. B* **572**, 152 (2003).
 - [15] J. M. Lattimer and Y. Lim, *Astrophys. J.* **771**, 51 (2013).
 - [16] F. J. Fattoyev and J. Piekarewicz, *Phys. Rev. Lett.* **111**, 162501 (2013).
 - [17] W. Nazarewicz, P.-G. Reinhard, W. Satula, and D. Vretenar, *Eur. Phys. J. A* **50**, 20 (2014).
 - [18] M. Kortelainen, J. Erler, W. Nazarewicz, N. Birge, Y. Gao, and E. Olsen, *Phys. Rev. C* **88**, 031305(R) (2013).
 - [19] X. Roca-Maza, M. Brenna, B. K. Agrawal, P. F. Bortignon, G. Colò, L.-G. Cao, N. Paar, and D. Vretenar, *Phys. Rev. C* **87**, 034301 (2013).
 - [20] A. Meucci, M. Vorabbi, C. Giusti, and P. Finelli, *Phys. Rev. C* **90**, 027301 (2014).
 - [21] J. D. McDonnell, N. Schunck, D. Higdon, J. Sarich, S. M. Wild, and W. Nazarewicz, *Phys. Rev. Lett.* **114**, 122501 (2015).
 - [22] T. Inakura and H. Nakada, *Phys. Rev. C* **92**, 064302 (2015).
 - [23] C. Mondal, B. K. Agrawal, and J. N. De, *Phys. Rev. C* **92**, 024302 (2015).
 - [24] M. Bender, P.-H. Heenen, and P.-G. Reinhard, *Rev. Mod. Phys.* **75**, 121 (2003).
 - [25] F. J. Fattoyev and J. Piekarewicz, *Phys. Rev. C* **84**, 064302 (2011).
 - [26] P.-G. Reinhard and W. Nazarewicz, *Phys. Rev. C* **87**, 014324 (2013).
 - [27] P.-G. Reinhard, J. Piekarewicz, W. Nazarewicz, B. K. Agrawal, N. Paar, and X. Roca-Maza, *Phys. Rev. C* **88**, 034325 (2013).
 - [28] Y. Gao, J. Dobaczewski, M. Kortelainen, J. Toivanen, and D. Tarpanov, *Phys. Rev. C* **87**, 034324 (2013).
 - [29] J. Dobaczewski, W. Nazarewicz, and P.-G. Reinhard, *J. Phys. G* **41**, 074001 (2014).
 - [30] S. Goriely and R. Capote, *Phys. Rev. C* **89**, 054318 (2014).
 - [31] J. Erler and P.-G. Reinhard, *J. Phys. G* **42**, 034026 (2015).
 - [32] M. Kortelainen, *J. Phys. G* **42**, 034021 (2015).
 - [33] J. Piekarewicz, W.-C. Chen, and F. J. Fattoyev, *J. Phys. G* **42**, 034018 (2015).
 - [34] X. Roca-Maza, N. Paar, and G. Colò, *J. Phys. G* **42**, 034033 (2015).
 - [35] P.-G. Reinhard, *Phys. Scr.* **91**, 023002 (2015).
 - [36] P. Klüpfel, P.-G. Reinhard, T. J. Bürvenich, and J. A. Maruhn, *Phys. Rev. C* **79**, 034310 (2009).
 - [37] P. Klüpfel, J. Erler, P.-G. Reinhard, and J. A. Maruhn, *Eur. Phys. J. A* **37**, 343 (2008).
 - [38] J. Friedrich and N. Vögler, *Nucl. Phys. A* **373**, 192 (1982).
 - [39] J. Friedrich and P.-G. Reinhard, *Phys. Rev. C* **33**, 335 (1986).
 - [40] P.-G. Reinhard and H. Flocard, *Nucl. Phys. A* **584**, 467 (1995).
 - [41] S. Brandt, *Statistical and computational methods in data analysis* (Springer-Verlag, New York, 1997).
 - [42] P.-G. Reinhard, M. Bender, W. Nazarewicz, and T. Vertse, *Phys. Rev. C* **73**, 014309 (2006).
 - [43] A. Ekström, G. R. Jansen, K. A. Wendt, G. Hagen, T. Papenbrock, B. D. Carlsson, C. Forssén, M. Hjorth-Jensen, P. Navrátil, and W. Nazarewicz, *Phys. Rev. C* **91**, 051301(R) (2015).